

# 3D non-linear time domain FEM-BEM approach to soil-structure interaction problems

A. Romero, P. Galvín, J. Domínguez

*Escuela Técnica Superior de Ingeniería, Universidad de Sevilla, Camino de los Descubrimientos, 41092 Sevilla, Spain*

---

## Abstract

Dynamic soil-structure interaction is concerned with the study of structures supported on flexible soils and subjected to dynamic actions. Methods combining the finite element method (FEM) and the boundary element method (BEM) are well suited to address dynamic soil-structure interaction problems. Hence, FEM-BEM models have been widely used. However, non-linear contact conditions and non-linear behaviour of the structures have not usually been considered in the analyses. This paper presents a 3D non-linear time domain FEM-BEM numerical model designed to address soil-structure interaction problems. The BEM formulation, based on element subdivision and the constant velocity approach, was improved by using interpolation matrices. The FEM approach was based on implicit Green's functions and non-linear contact was considered at the FEM-BEM interface. Two engineering problems were studied with the proposed methodology: the propagation of waves in an elastic foundation and the dynamic response of a structure to an incident wave field.

*Key words:* soil-structure interaction, FEM-BEM coupling, time domain, non-linear

---

## 1. Introduction

Dynamic soil-structure interaction (SSI) is concerned with the study of structures supported on flexible soils and subjected to dynamic actions. Vibrations of machines on elastic foundations, vibrations induced by traffic and structures in seismic areas are examples of problems where SSI plays an important role. In all of the above examples, the flexibility of the soil has an important effect on the response of the structure and should be taken into account in the analysis. Methods combining the finite element method (FEM) and the boundary element method (BEM) are well suited to address dynamic soil-structure interaction problems. Boundless regions such as soils are naturally represented by the BEM, since the radiation of waves towards infinity is automatically included in the model [1]. The FEM is especially useful to study structures considering their non-linear behaviour.

---

*Email address:* [pedrogalvin@us.es](mailto:pedrogalvin@us.es) (P. Galvín)

BEM or FEM-BEM models have been used, for example, to compute the dynamic stiffness of foundations in the frequency domain [2], to study soil-dam-reservoir systems by 2D [3, 4] and 3D [5] frequency domain models, to analyse foundation systems in layered [6] and homogeneous [7, 8, 9] soil media and to predict traffic-induced vibration by wavenumber-frequency approaches [10, 11, 12]. However, non-linear contact conditions and non-linear behaviour of the structures have not usually been considered in the analyses. SSI problems in which non-linear effects are important require a direct time domain approach.

In recent years, several authors have developed and applied 3D time domain FEM-BEM methods to solve elastodynamic problems [13]. Some of the following papers are based on the formulation presented by Mansur [14]. This formulation can be used to take into account the actual geometry of the elements studied and their non-linear behaviour. Karabalis and Beskos [15, 16] computed the dynamic response of rigid and flexible foundations. Kontini et al. [17] presented an approximate methodology and analysed the response of a cavity embedded in a semi-infinite medium under the influence of external forces and seismic waves. Schanz studied the wave propagation in poroelastic solids [18]. Rizos and his co-workers [19, 20] presented a coupled methodology and computed the cross-interaction of square foundations and high speed train induced vibrations. Marrero and Domínguez [21] studied a plate with a central crack with a nonuniform mesh. Galvín et al. [22, 23, 24, 25] presented a comprehensive train-track-soil-structure model and studied vibrations induced by train passage on ballast and non-ballast tracks and the resonant response of railway bridges. However, 3D time domain models also have some disadvantages: they are computationally expensive and certain issues related to stability, coupling and efficiency have not been satisfactorily solved yet.

Regarding stability, time domain models have shown problems with some combinations of spatial and temporal discretizations [26, 27]. The dynamic analysis of finite and semi-infinite domains involves the existence of two kinds of waves in the fundamental solution. Hence, the multiple reflection of different kinds of waves on the boundaries may lead to causality errors and instability problems. Several studies have attempted to improve the stability and causality of BEM approaches. Mansur and his co-workers [28, 29, 30, 31] developed two algorithms for improving the stability of the time response: the  $\theta$  time-marching scheme and the time-weighted method. In the  $\theta$  scheme [28, 29, 30] the response at the corresponding time is firstly evaluated at a slightly longer time. The time weighting method [31] averages the whole time history of the solution in a weighted residual sense. Peirce and his co-workers [32, 33] presented the  $\varepsilon$  scheme, as the  $\theta$  scheme, based on increased the time step. Marrero and Domínguez [21] used a linear combination of equations for several time steps to advance one step and applied element subdivision to numerical integration to improve stability in time.

FEM and BEM can be coupled directly by assembling the equations obtained from both methods into a global system of equations. Equilibrium and displacement compatibility are established at nodes on the FEM-BEM interfaces [23, 34, 35, 36]. In this case, the procedure for merging the equations can be complicated and the system of equations is larger than the uncoupled FEM or BEM systems. Alternatively,

either staggered [19] or iterative methods have been developed to overcome these difficulties, allowing separate analysis of both methods. Von Estorff and Hagen [37] presented a FEM-BEM model for the transient analysis of wave propagation problems, where the coupling of the methods was performed in an iterative manner by an interface relaxation method. The previous model is an extension of the work by Soares et al. [38]. The iterative coupling algorithms involve a much smaller system of equations than the conventional coupled system. Specialized solvers can be used to solve the system of equations according to their special characteristics. It is also possible to use different time steps for every method. The convergence of these algorithms is influenced by the selection of the time step of each method and the choice of the iterative coupling relaxation parameter [39, 40, 41]. Lastly, Soares Jr. et al. [42] have presented a formulation that avoids the iterative procedures but considers the FEM and BEM separately. Therefore, it retains most of the advantages of the iterative coupling approach.

The efficiency of the model can be improved by reducing computational effort. It is highly time consuming to compute the full unsymmetrical boundary element system matrices and the convolution derived from previous steps. However, the 3D time domain BEM can be accelerated by truncating the time convolution process [43, 44].

In this study, previous ideas presented in 2D models [42, 45, 46, 47] were used to develop a 3D non-linear time domain FEM-BEM numerical model to address soil-structure interaction problems. The BEM formulation, based on element subdivision and the constant velocity approach [21], was improved by employing interpolation matrices to compute time-domain influence matrices. The FEM approach was based on implicit Green's functions and non-linear contact was considered at the FEM-BEM interface. Thus, this methodology accounts for any uplifting or other contact effects.

The outline of this paper is as follows. The first section presents the BEM approach and assesses its improvements. The second section summarizes the FEM methodology and the non-linear FEM-BEM coupling. Non-linear coupling was based on Kuhn-Tucker constraints [48]. The last section analyses two numerical examples: the propagation of waves in an elastic foundation and the dynamic response of a structure to an incident wave field.

## 2. Boundary element approach

The 3D time domain boundary element (BE) formulation for transient problems is briefly summarized in this section. This topic is addressed more thoroughly in Domínguez [1].

The integral representation of the displacement  $u$  at a point  $i$  on the boundary  $\Gamma$  of an elastic body at time  $t$  with zero body forces and zero initial conditions can be written as:

$$c_{lk}^i u_k^i(\mathbf{x}^i, t) = \int_0^{t^+} \int_{\Gamma} u_{lk}(\mathbf{x}, t - \tau; \mathbf{x}^i) p_k(\mathbf{x}, \tau) d\Gamma(\mathbf{x}) d\tau - \int_0^{t^+} \int_{\Gamma} p_{lk}(\mathbf{x}, t - \tau; \mathbf{x}^i) u_k(\mathbf{x}, \tau) d\Gamma(\mathbf{x}) d\tau \quad (1)$$

where  $u_k$  and  $p_k$  stand for the  $k$  component of the displacement and traction, respectively;  $u_{lk}(\mathbf{x}, t - \tau; \mathbf{x}^i)$  and  $p_{lk}(\mathbf{x}, t - \tau; \mathbf{x}^i)$  are the full-space fundamental solution displacement and traction tensors, respectively, at point  $\mathbf{x}$  due to a point load at  $\mathbf{x}^i$ . The coefficient  $c_{lk}^i$  depends only on the boundary geometry at point  $i$ . Displacements and tractions over the boundary are approximated from their nodal values at each time step  $m$ ,  $u_k^{mj}$  and  $p_k^{mj}$ , using the space interpolation functions  $\phi^j(r)$  and  $\psi^j(r)$  and the time interpolation functions  $\eta^m(\tau)$  and  $\mu^m(\tau)$ .

After interpolating the boundary variables, Equation (1) at time  $t = n\Delta t$  becomes:

$$c_{lk}^i u_k^{ni} = \sum_{m=1}^n \sum_{j=1}^Q \left[ \left\{ \int_{\Gamma_j} \left[ \int_{\Delta t_m} u_{lk} \mu^m d\tau \right] \psi^j d\Gamma \right\} p_k^{mj} - \left\{ \int_{\Gamma_j} \left[ \int_{\Delta t_m} p_{lk} \eta^m d\tau \right] \phi^j d\Gamma \right\} u_k^{mj} \right] \quad (2)$$

where  $Q$  is the total number of boundary nodes and  $\Gamma_j$  represents the elements to which node  $j$  belongs. The integrals of  $u_{lk} \mu^m$  and  $p_{lk} \eta^m$  for each time step are usually called  $U_{lk}^{nm}$  and  $P_{lk}^{nm}$ , respectively.

Thus, Equation (2) becomes:

$$c_{lk}^i u_k^{ni} = \sum_{m=1}^n \sum_{j=1}^Q \left[ \left\{ \int_{\Gamma_j} U_{lk}^{nm} \psi^j d\Gamma \right\} p_k^{mj} - \left\{ \int_{\Gamma_j} P_{lk}^{nm} \phi^j d\Gamma \right\} u_k^{mj} \right] \quad (3)$$

which in a more compact form can be written as:

$$c_{lk}^i u_k^{ni} = \sum_{m=1}^n \sum_{j=1}^Q \left[ G_{lk}^{nmij} p_k^{mj} - \hat{H}_{lk}^{nmij} u_k^{mj} \right] \quad (4)$$

Once the independent term  $c_{lk}^i$  is included in the system matrix, the integral representation for point  $i$  at time  $t = n\Delta t$  becomes:

$$\sum_{m=1}^n \sum_{j=1}^Q H_{lk}^{nmij} u_k^{mj} = \sum_{m=1}^n \sum_{j=1}^Q G_{lk}^{nmij} p_k^{mj} \quad (5)$$

and the system of equations for all the boundary nodes at time  $t = n\Delta t$  can be written in matrix form as:

$$\mathbf{H}^{nn} \mathbf{u}^n = \mathbf{G}^{nn} \mathbf{p}^n + \sum_{m=1}^{n-1} (\mathbf{G}^{nm} \mathbf{p}^m - \mathbf{H}^{nm} \mathbf{u}^m) \quad (6)$$

Once the boundary conditions are applied, Equation (6) yields a system of equations that can be solved step by step to obtain the time variation of the boundary unknowns.

Piecewise constant time interpolation functions  $\mu^m(\tau)$  were used for tractions and piecewise linear functions  $\eta^m(\tau)$  were used for displacements. The time integrals in Equation (2) can be evaluated analytically without much difficulty.

In the present model, nine-node quadratic elements are used. Each side of the element is divided into equal parts in the natural coordinates domain yielding and element subdivision. The spatial integration extends only to those subdivisions, which mid-point is under the effects of the fundamental solution waves according to the causality condition of each term of the fundamental solution. The subsequent integration

over each subdivision is done using a standard  $2 \times 2$  Gauss quadrature always that the collocation point does not belong to the subdivision, independently of whether it belongs to the same element or it does not. The subdivision containing the collocation point are under the effects of non-zero fundamental solution terms only when  $n = m$ . In that case a peak singularity of the type  $1/r$  appears in the fundamental solution displacement, and a strong singularity of the type  $1/r^2$  appears in the fundamental solution traction. Both integrals containing singularities are evaluated in a direct form [21]. No enclosing elements are needed in unbounded domains to carry out the so-called rigid body motion procedure. The coefficient  $c_{lk}^i$  is computed using the methodology presented in references [49, 50].

As mentioned above, ensuring a stable stepping procedure is an important issue in time domain BEM. An approach based on the idea of using a linear combination of equations for several time steps in order to advance one step was applied [21]. Equation (6) became:

$$\begin{aligned} & \left\{ 4\mathbf{H}^{nn} + \mathbf{H}^{(n+1)n} \right\} \mathbf{u}^n = \left\{ 4\mathbf{G}^{nn} + \mathbf{G}^{(n+1)n} \right\} \mathbf{p}^n + \mathbf{H}^{nn} \mathbf{u}^{(n-1)} - \mathbf{G}^{nn} \mathbf{p}^{(n-1)} \\ & + \sum_{m=1}^{n-1} \left\{ \left( \mathbf{G}^{(n+1)m} + 2\mathbf{G}^{nm} + \mathbf{G}^{(n-1)m} \right) \mathbf{p}^m - \left( \mathbf{H}^{(n+1)m} + 2\mathbf{H}^{nm} + \mathbf{H}^{(n-1)m} \right) \mathbf{u}^m \right\} \end{aligned} \quad (7)$$

To reduce computational effort, the formulation presented by Soares and Mansur [44] for 2D problems was extended to 3D analysis in the present study. The boundary element system matrices  $\mathbf{H}^{nm}$  and  $\mathbf{G}^{nm}$  depend on the difference  $(n - m)$  rather than on the values of  $n$  and  $m$ . These matrices were interpolated by  $k$  interpolating matrices  $\mathbf{H}_j$  and  $\mathbf{G}_j$  to compute influence matrices that appeared at the convolutions in Equation (7) when  $(n - m)\Delta t$  exceeded a threshold time  $T_L = L\Delta t$ . The kernels  $U_{lk}^{nm}$  and  $P_{lk}^{nm}$  of these integrals consisted of terms due to waves propagating with velocity  $c_p$  (P-waves) and terms due to waves propagating with velocity  $c_s$  (S-waves). Each of these terms was different from zero only in those parts of a given element that were under the effects of the waves leaving the collocation point during the time interval  $(n - m)\Delta t \geq t \geq [n - (m + 1)]\Delta t$ . That is, the parts of the element between two spherical surfaces of radius  $r_m = c(n - m)\Delta t$  and  $r_{m+1} = c[n - (m + 1)]\Delta t$ , with  $c = c_p$  or  $c = c_s$  depending on the term. As  $r_{max}$  was the maximum distance between the collocation point and any element in the discretization and  $c_s$  was the minimum wave velocity, from time  $T_N = N\Delta t = r_{max}/c_s$  approximately, the kernels  $U_{lk}^{nm}$  and  $P_{lk}^{nm}$  were equal to zero.

Equation (7) was rewritten accounting for the interpolation of the time convolution process and the

stability improvement. After that, the upper index of the matrices indicated the difference  $(n - m + 1)$ :

$$\begin{aligned}
& \{4\mathbf{H}^1 + \mathbf{H}^2\} \mathbf{u}^n = \{4\mathbf{G}^1 + \mathbf{G}^2\} \mathbf{p}^n - \left( \mathbf{G}^1 \mathbf{p}^{(n-1)} - \mathbf{H}^1 \mathbf{u}^{(n-1)} \right) \\
& + \sum_{m=1}^{L-1} \left\{ \mathbf{G}^m (\mathbf{p}^{n-m+2} + 2\mathbf{p}^{n-m+1} + \mathbf{p}^{n-m}) - \mathbf{H}^m (\mathbf{u}^{n-m-2} + 2\mathbf{u}^{n-m+1} + \mathbf{u}^{n-m}) \right\} \\
& + \sum_{m=L}^{n-1} \left\{ \sum_{j=1}^k [\mathbf{G}_j I(m, j)] (\mathbf{p}^{n-m+2} + 2\mathbf{p}^{n-m+1} + \mathbf{p}^{n-m}) - \sum_{j=1}^k [\mathbf{H}_j I(m, j)] (\mathbf{u}^{n-m-2} + 2\mathbf{u}^{n-m+1} + \mathbf{u}^{n-m}) \right\}
\end{aligned} \tag{8}$$

The interpolation coefficients  $I(m, j)$  can be computed according to Chebyshev-Lagrange (Equation (9)) or multi-linear (Equation (10)) approaches:

$$I(m, j) = \prod_{i=1, i \neq j}^k \frac{m\Delta t - T_i}{T_j - T_i} \tag{9}$$

$$I(m, j) = \frac{T_{j+1} - m\Delta t}{T_{j+1} - T_j} \quad m\Delta t \in [T_j, T_{j+1}] \tag{10}$$

where interpolation time steps  $T_j$  for Chebyshev-Lagrange (Equation 11) and multi-linear (Equation 12) approaches are:

$$T_j = \frac{1}{2} \left[ (T_N - T_L) \cos \left( \frac{2j-1}{2k} \pi \right) + (T_N + T_L) \right] \quad j = 1, \dots, k \tag{11}$$

$$T_j = T_L + (T_N - T_L) \left( \frac{j-1}{k-1} \right)^{k^p} \quad j = 1, \dots, k \tag{12}$$

### 2.1. Verification example

The BEM technique summarized previously was used to study the motion of the surface of a uniform elastic half-space caused by applying a point load  $p(t) = p_0 H(t)$  that varied with time as a Heaviside function. This problem was analytically studied by Pekeris [51], who obtained vertical and horizontal displacements at the surface for a Poisson's ratio  $\nu = 0.25$  (i.e. for the same Lamé constants  $\mu$  and  $\lambda$ ). Later, Rizos and Karabalis computed the vertical displacement with a time domain BEM based on B-spline fundamental solutions [52].

The half-space surface was discretized into quadrilateral nine-node elements as shown in Figure 1. A surface of  $36 \text{ m} \times 36 \text{ m}$  was represented by 1296 elements. The wave propagation velocities of the half-space were taken as  $c_p = 548 \text{ m/s}$  and  $c_s = 316 \text{ m/s}$ . Additionally, a density  $\rho = 2000 \text{ kg/m}^3$  was assumed for the half-space. The time step for the boundary element analysis was set as  $\Delta t = 7.5 \times 10^{-4} \text{ s}$ . The stability parameter  $\beta = c\Delta t/l$ , where  $l$  is the distance between two nodes of an element, takes values  $0.3 < \beta < 0.8$ . Figure 2 shows vertical half-space surface dimensionless displacements  $\tilde{u}(t) = \pi\mu u(t)r/p_0$  at two time steps, where  $r$  is the distance from the observation point to the load axis. The results showed a radial symmetry about the point load and diffraction or refraction effects were not noticeable.

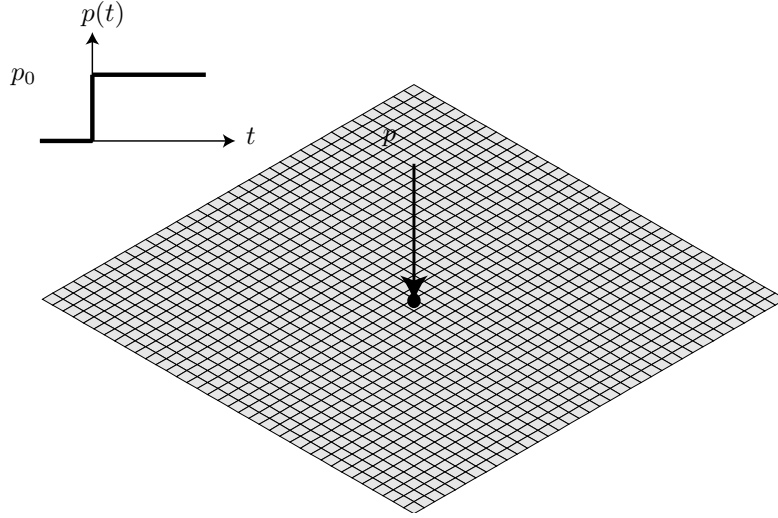


Figure 1: Half-space discretization

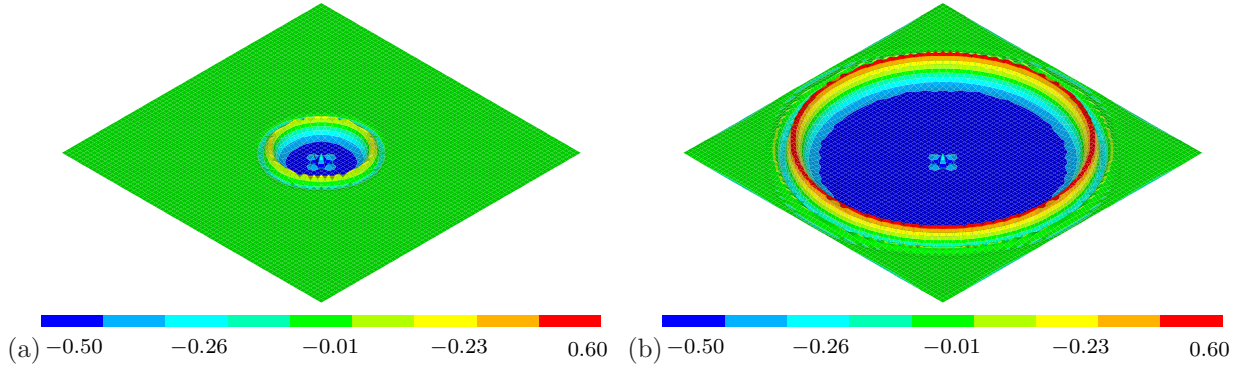


Figure 2: Vertical half-space surface dimensionless displacements  $\tilde{u} = \pi\mu u(t)r/p_0$  at (a)  $t = r/c_s = 5 \text{ m}/316 \text{ m/s} = 0.0158 \text{ s}$  and (b)  $t = r/c_s = 15 \text{ m}/316 \text{ m/s} = 0.0474 \text{ s}$

Figures 3 and 4 show horizontal and vertical dimensionless displacement versus dimensionless time  $\tau = c_s t/r$  at two points located at  $r = 5 \text{ m}$  and  $r = 15 \text{ m}$ , respectively. Both analytical and numerical results were compared. Pekeris' analytical solution [51] presents a perturbation when the P wave arrived at the observation point ( $\tau = 0.57$ ) and became infinite upon the arrival of the Rayleigh wave ( $\tau = 1.08$ ). In the numerical model the analytical response was only partially reproduced since the load was distributed according to element shape functions. The maximum response was computed at a time between the arrivals of the S wave ( $\tau = 1.00$ ) and the Rayleigh wave. As the  $r$  distance increased, the numerical result tended to the analytical solution. Figures 3 and 4 also show computed displacements when the boundary element matrices were interpolated by multi-linear (ML) and Chebyshev-Lagrange (CL) approaches from times  $\tau_L = c_s T_L/r = 0.5, 1$  and  $1.5$ . The number  $k$  of interpolating matrices was set for computing exact matrices ( $\mathbf{H}_j$  and  $\mathbf{G}_j$ ) every 5 time steps. Table 1 presents saved CPU time and memory and error when the interpolated

BEM formulation was used. At  $r = 5$  m a considerably good correlation between non-interpolated and interpolated formulations was obtained for  $\tau_L = 1.5$ , saving 71% CPU time and about 62% CPU memory compared to the non-interpolated formulation. As the dimensionless threshold time  $\tau_L$  decreased, error increased because the correlation dropped at  $\tau$  higher than  $\tau_L$  in both multi-linear and non-equidistant Chebyshev approaches. At  $r = 15$  m, since the distance from the load point increased, the arrival time of the S wave increased and saved CPU time and memory decreased. A good correlation was obtained for  $\tau_L = 1.5$ , saving 15% CPU time and about 17% CPU memory. In this case, the computational time to solve Equation (8) on a computer with 8 cores at 3.4 GHz processor was about 25 minutes.

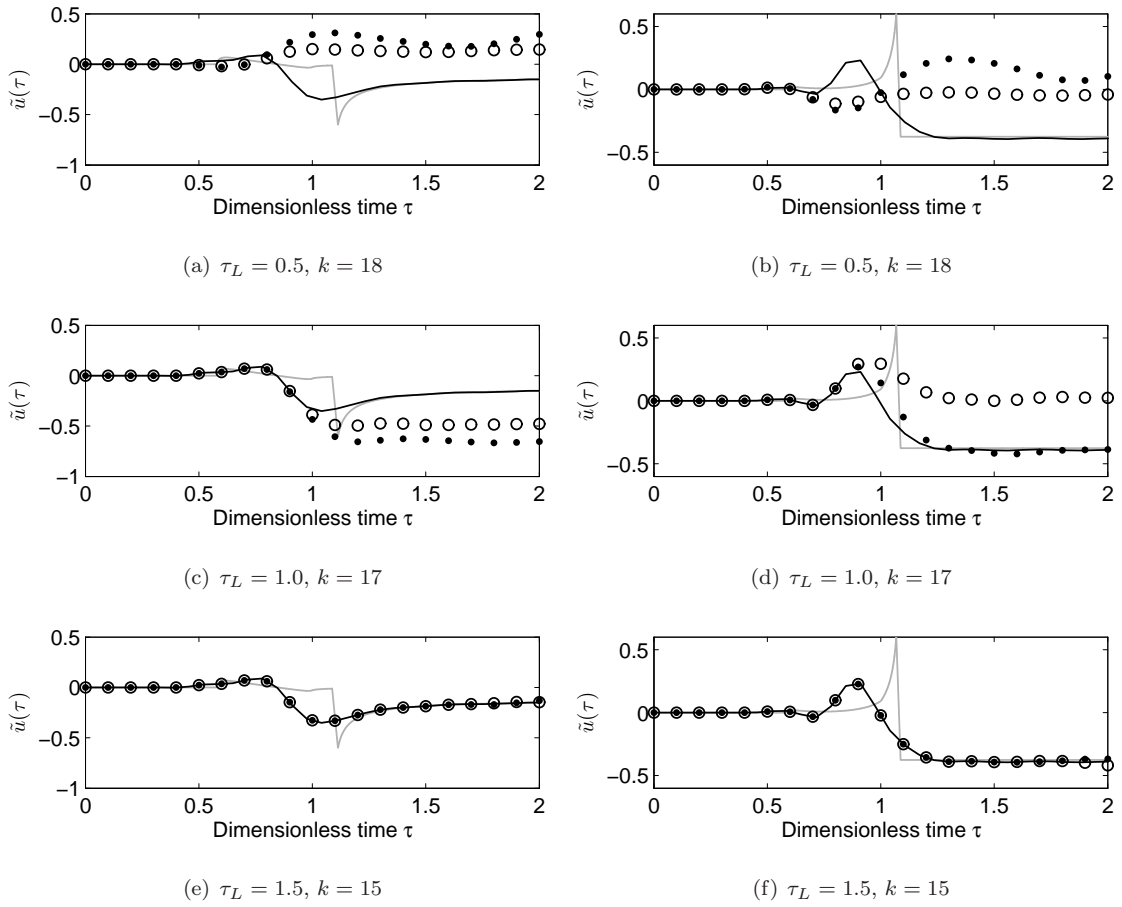


Figure 3: (a,c,e) Horizontal and (b,d,f) vertical dimensionless displacement at  $r = 5$  m. Pekeris' analytical solution (grey line), non-interpolated BEM (black line), multi-linear interpolated BEM (black dot) and Chebyshev-Lagrange interpolated BEM (black circle).

Figures 5 and 6 show the time histories of the matrix elements  $H_{lk}^{ij}$  and  $G_{lk}^{ij}$ . The results presented above depend on these elements, as shown by the convolutions in Equation (8). Very good approximations of the  $\mathbf{H}^m$  and  $\mathbf{G}^m$  matrices were obtained for  $\tau_L = 1.5$ . However, appreciable differences appeared as the interpolation time zone was higher. The error increased when the threshold time was far from the arrival

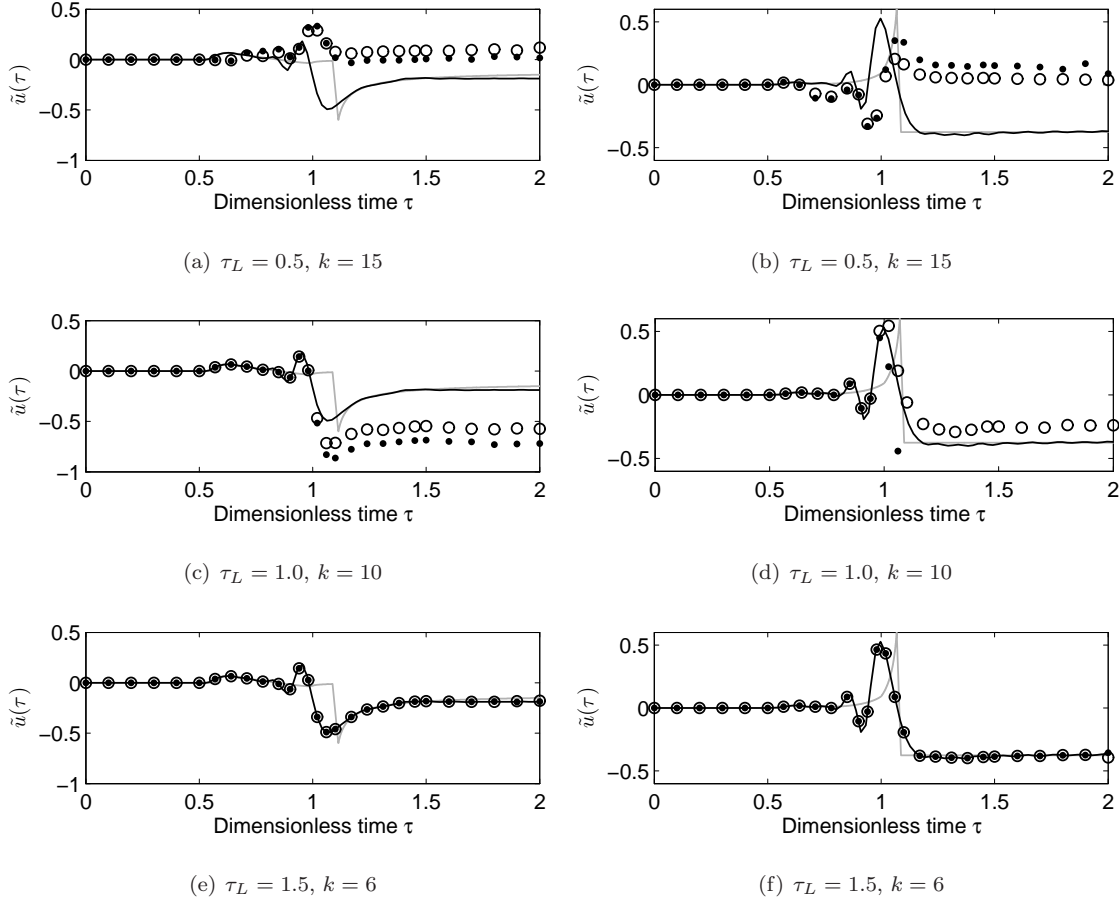


Figure 4: (a,c,e) Horizontal and (b,d,f) vertical dimensionless displacement at  $r = 15$  m. Pekeris' analytical solution (grey line), non-interpolated BEM (black line), multi-linear interpolated BEM (black dot) and Chebyshev-Lagrange interpolated BEM (black circle).

time of the S wave. Based on a more extensive parametric study, it was concluded that the interpolation of the time convolution process is valid when  $\tau_L$  is higher than  $\tau = 1.08$ . This means when it is higher than the arrival time of the Rayleigh wave so that the approximation of the time convolution process does not significantly modify the wave propagation problem.

### 3. Finite element formulation based on implicit Green's function

Dynamic analysis of structures using Green's functions is usually performed with modal coordinates. This technique decouples the system of equations in a set of independent equations of a single degree of freedom [53]. Analysis of dynamic systems in nodal coordinates is limited by the existence of analytical Green's functions and involves a high computational cost. Numerical calculation of the explicit Green's functions of a system is only suitable for simplified models.

Table 1: Interpolated BEM formulation: error and saved CPU time and memory.

		$r = 5$ m			$r = 15$ m		
	$\tau_L = T_L c_S / r$	0.5	1	1.5	0.5	1	1.5
	$k$	18	17	15	15	10	6
ML	Vertical displacement error (%)	72.5	8.1	1.3	85.5	71.0	0.4
	Horizontal displacement error (%)	73.4	9.4	0.8	83.8	68.5	0.2
	Saved CPU time (%)	80	76	71	71	54	15
	Saved CPU memory (%)	76	71	65	65	53	19
CL	Vertical displacement error (%)	55.3	47.2	0.6	58.4	15.2	0.7
	Horizontal displacement error (%)	59.6	47.3	0.8	59.3	16.7	0.6
	Saved CPU time (%)	79	75	71	71	54	15
	Saved CPU memory (%)	76	72	62	65	62	17

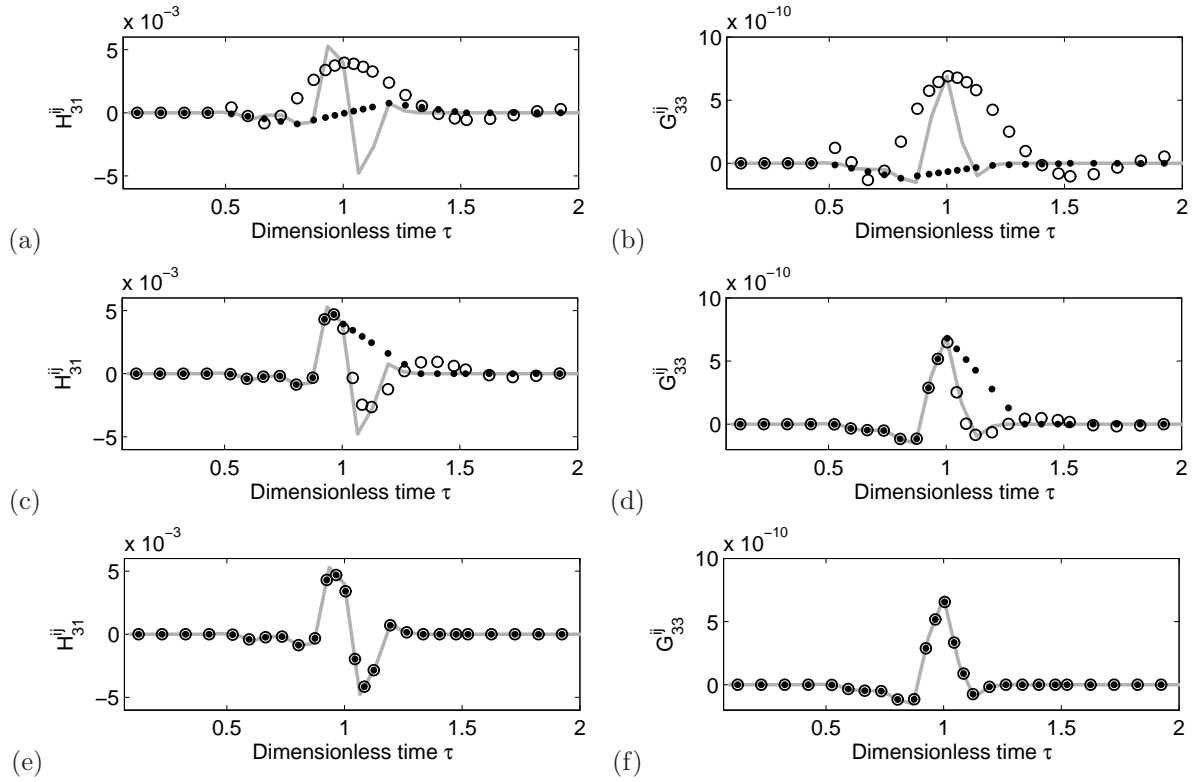


Figure 5: Time history of the matrix elements (a,c,e)  $H_{31}^{ij}$  and (b,d,f)  $G_{33}^{ij}$  at  $x^i(r = 0)$ ,  $x^j(r = 5)$ . Non-interpolated BEM (grey line), multi-linear interpolated BEM (black dot) and Chebyshev-Lagrange interpolated BEM (black circle).

Soares and Mansur [45] recently presented a finite element formulation based on implicit Green's functions. The Green's functions of the system and their time derivatives are obtained implicitly applying

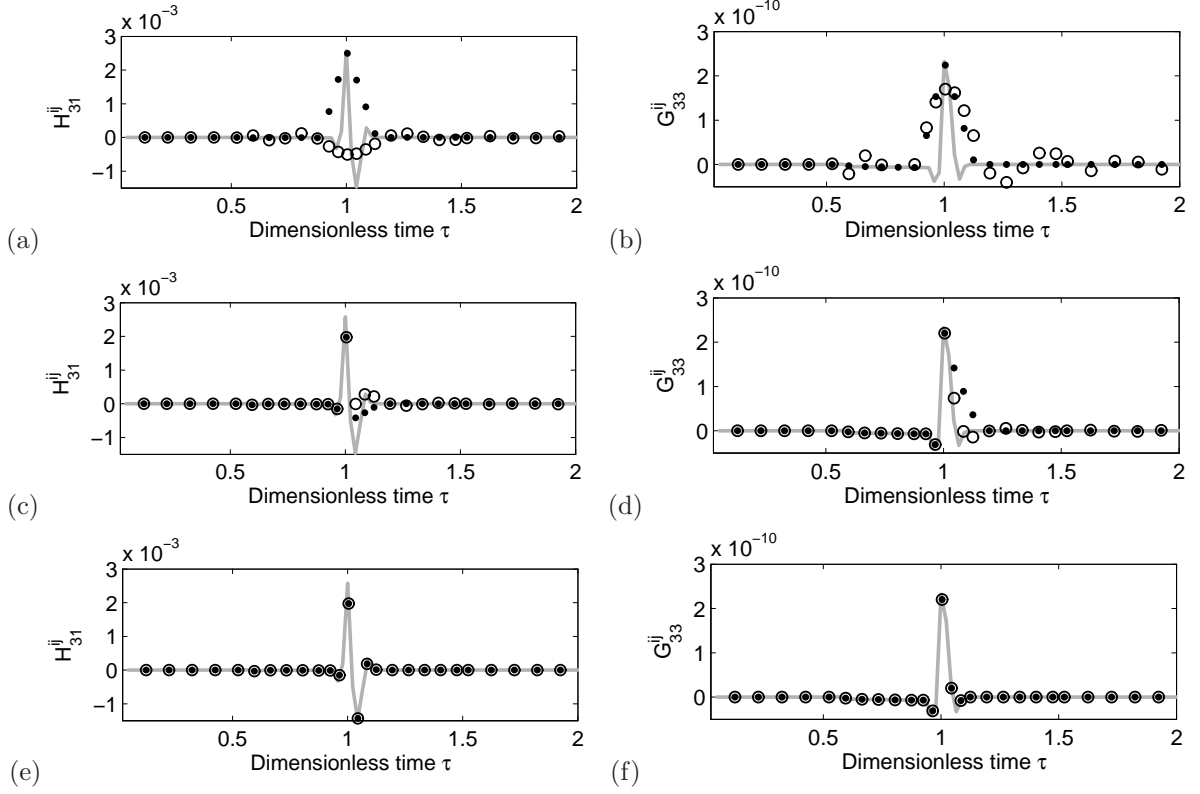


Figure 6: Time history of the matrix elements (a,c,e)  $H_{31}^{ij}$  and (b,d,f)  $G_{33}^{ij}$  at  $\mathbf{x}^i(r=0)$ ,  $\mathbf{x}^j(r=15)$ . Non-interpolated BEM (grey line), multi-linear interpolated BEM (black dot) and Chebyshev-Lagrange interpolated BEM (black circle).

Newmark's method. Displacements and velocities at time  $t = n\Delta t$  are as follows:

$$\mathbf{u}^n = \mathbf{D}^{-1}\mathbf{M}(b_4\mathbf{u}^{n-1} + b_1\dot{\mathbf{u}}^{n-1}) + b_2\mathbf{u}^{n-1} \quad (13)$$

$$\dot{\mathbf{u}}^n = b_7\mathbf{D}^{-1}\mathbf{M}(b_4\mathbf{u}^{n-1} + b_1\dot{\mathbf{u}}^{n-1}) + b_6\mathbf{u}^{n-1} + b_2\dot{\mathbf{u}}^{n-1} + \mathbf{f}^{n*} \quad (14)$$

where  $\mathbf{M}$  is the mass matrix,  $\mathbf{D}$  the dynamic stiffness matrix:

$$\mathbf{D} = \frac{1}{\alpha\Delta t^2}\mathbf{M} + \frac{\delta}{\alpha\Delta t}\mathbf{C} + \mathbf{K} \quad (15)$$

$\mathbf{C}$  and  $\mathbf{K}$  are the damping and the stiffness matrices, respectively, and  $\mathbf{f}^{n*}$  is the effective force. These expressions are valid assuming that the damping matrix is proportional to the mass matrix by the parameter  $\alpha_m$  ( $\mathbf{C} = \alpha_m\mathbf{M}$ ) and the integration constants satisfy the trapezoidal rule ( $\delta^2 = \alpha$ ). The time integration procedure is unconditionally stable and second-order accurate if Newmark's parameters are  $\alpha = 0.25$  and  $\beta = 0.5$  [45]. The effective force is given by:

$$\mathbf{f}^{n*} = \mathbf{M}^{-1}\mathbf{f}^n\Delta t \quad (16)$$

where  $\mathbf{f}^n$  is the applied force at time step  $n$ . In Equation (16) the mass matrix inverse is required to compute the effective force. The computational cost of matrix inversion is considerably reduced if it is diagonalized.

The constants in Equations (13) and (14) are:

$$b_0 = \left( \frac{1}{2\alpha} - 1 \right) \alpha_m - \frac{1}{\alpha \Delta t} \quad (17)$$

$$b_1 = \left( \frac{\delta}{\alpha} - 1 \right) \alpha_m - \left( \frac{\Delta t}{2} \right) \left( \frac{\delta}{\alpha} - 2 \right) \alpha_m^2 - b_0 \quad (18)$$

$$b_2 = 1 - \Delta t(1 - \delta)\alpha_m + \delta \Delta t b_0 \quad (19)$$

$$b_3 = \frac{\delta b_1}{\alpha \Delta t} \quad (20)$$

$$b_4 = \alpha_m b_1 + b_3 \quad (21)$$

$$b_5 = \alpha_m b_3 + \frac{b_1}{\alpha \Delta t^2} \quad (22)$$

$$b_6 = \alpha_m b_2 + b_0 \quad (23)$$

$$b_7 = b_3/b_1 \quad (24)$$

#### 4. Non-linear FEM-BEM coupling

Next, a non-linear coupling method is presented to account for uplifting or other contact effects in SSI problems. Contact analysis involves the resolution of a non-linear minimization problem subjected to Kuhn-Tucker constraints at the interface [48]. The proposed algorithm is based on the evaluation of Kuhn-Tucker constraints at time step  $n$ :

$$g_N^n \geq 0, \quad -p_N^n + p_C \geq 0, \quad (-p_N^n + p_C) g_N = 0 \quad (25)$$

where  $g_N^n$  is the normal gap between the soil and the structure,  $p_N^n$  represents the normal traction on the interface surface, and  $p_C$  is the cohesion limit that allows for considering cohesive effects.

Finite element displacement  $\mathbf{u}^n$  at time step  $n$  (Equation (13)) depends on displacement and velocity at previous time steps  $\mathbf{u}^{n-1}$  and  $\dot{\mathbf{u}}^{n-1}$ , respectively, but it does not depend on  $\mathbf{f}^n$ . Therefore, FEM and BEM equations can be decoupled and solved separately [42]. Next, the coupling of both methods is ensured by imposing compatibility and equilibrium conditions at the interface after evaluation of Kuhn-Tucker constraints (Equation (25)) at time step  $n$ :

$$\mathbf{u}_b^n = \mathbf{u}_f^n \quad (26)$$

$$\mathbf{f}_f^n = -\mathbf{f}_b^n \quad (27)$$

where  $f$  and  $b$  subscripts refer to interface nodes belonging to finite element and boundary element discretizations, respectively, and nodal force  $\mathbf{f}_b^n$  is obtained from nodal traction  $\mathbf{p}_b^n$ , as can be found in reference

[23]. Normal gap and normal traction at the interface surface are given by:

$$g_N^n = (\mathbf{u}_b^{n-1} - \mathbf{u}_f^n) \cdot \mathbf{n}_f \quad (28)$$

$$p_N^n = \mathbf{p}_b^n \cdot \mathbf{n}_b \quad (29)$$

where  $\mathbf{n}_f$  and  $\mathbf{n}_b$  are the external normals.

The proposed method can be used to solve dynamic contact problems efficiently and is quite simple to implement in standard BEM-FEM codes. Table 2 shows further details on the proposed algorithm.

---

Table 2: Algorithm for the solution of dynamic soil-structure interaction problems accounting for contact effects.

---

A *Initial settings:*

A.1 Compute BEM and FEM matrices ( $\mathbf{H}^n$ ,  $\mathbf{G}^n$ ,  $\mathbf{H}_j$ ,  $\mathbf{G}_j$  and  $\mathbf{D}$ ) and select interpolation procedure and  $T_j$  time steps.

B *For each time step  $n$ :*

B.1 Compute FEM displacement  $\mathbf{u}^n$  with Equation (13).

B.2 Evaluate Kuhn-Tucker constraints (Equation (28)) and establish compatibility condition (Equation (26)).

B.3 Solve BEM problem (Equation (8)).

B.4 Evaluate Kuhn-Tucker constraints (Equation (29)) and establish appropriate equilibrium condition (Equation (27)).

B.5 Compute effective force accounting for equilibrium condition  $\mathbf{f}^{n*} = \mathbf{M}^{-1}(\mathbf{f}^n + \mathbf{f}_f^n)\Delta t$ .

B.6 Compute FE velocity  $\dot{\mathbf{u}}^n$  (Equation (14)).

---

## 5. Numerical examples

In this section, two engineering problems are studied with the proposed numerical model. In the first case, the dynamic behaviour of a foundation is analysed accounting for non-linear soil-structure contact. The second case is an analysis of the dynamic response of a structure to an incident wave field.

### 5.1. Propagation of waves in an elastic foundation

The following is an analysis of the propagation of waves in an elastic foundation on a homogeneous soil. Similar studies have previously been conducted on linear [2, 15, 54] and non-linear [42, 55] behaviour. In this study, linear and non-linear soil-foundation contact models were taken into account in the computations. Thus, any uplifting or other contact effects can be considered by the proposed methodology.

Figure 7.(a) shows the problem geometry and the associated discretization. The soil was discretized using quadrilateral nine-node boundary elements. A length of  $L = 2.5$  m around the origin of the coordinate system was represented by 145 elements [1]. The soil was assumed to be an elastic half-space with the

following properties:  $c_p = 42 \text{ m/s}$ ,  $c_s = 20 \text{ m/s}$ ,  $c_R = 19 \text{ m/s}$  and  $\rho = 1800 \text{ kg/m}^3$ . The concrete foundation ( $1 \text{ m} \times 1 \text{ m} \times 0.5 \text{ m}$ ) was discretized by using 400 eight-node brick elements. The concrete properties were: Young's modulus  $E = 300 \times 10^6 \text{ N/m}^2$ , Poisson's ratio  $\nu = 0.2$  and density  $\rho = 2000 \text{ kg/m}^3$ . The bottom of the foundation was coupled to the soil. The top of the foundation was excited vertically by a pressure load according to  $p(t) = -p_0(H(t) - H(t - 0.025 \text{ s}))$  where  $p_0 = 1000 \text{ N/m}^2$ . Figures 7.(b)-(c) show the symmetrical and antisymmetrical load cases studied, respectively. The time step for the analysis was set at  $\Delta t = 6.25 \times 10^{-3} \text{ s}$ . The stability parameter  $\beta = c\Delta t/l$  takes values  $0.31 < \beta < 1.25$ . To reduce computational effort, the influence matrices were interpolated from  $T_L = \sqrt{2}L/c_R = 0.17 \text{ s}$  by  $k = 2$  interpolating matrices using a Chebyshev-Lagrange approach.

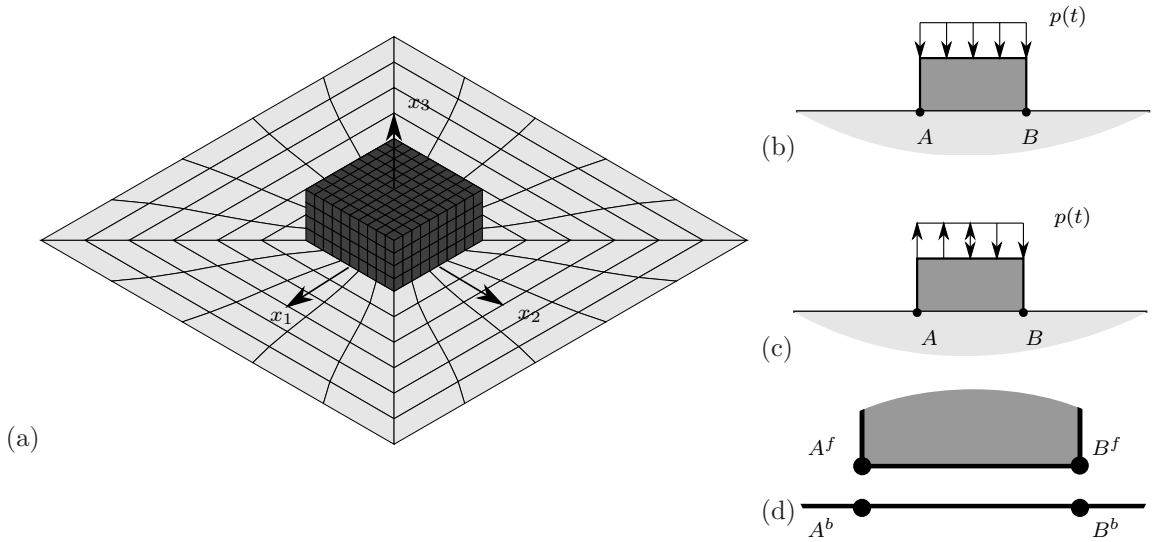


Figure 7: (a) Soil-foundation discretization and load cases: (b) symmetry and (c) antisymmetry.

Figure 8 shows the dimensionless response  $\tilde{u} = \pi\mu u(t)r/p_0$  of the soil-foundation system in the symmetrical load case accounting for linear and non-linear contact, where  $r = ((x_1 - x_{1i})^2 + (x_2 - x_{2i})^2)^{0.5}$  is the in-plane distance to the centre of the foundation ( $x_{1i} = 0$  and  $x_{2i} = 0$ ). Displacement compatibility depended on interface behaviour: a light uplifting was observed in Figure 8.(b), where an adhesive limit  $p_C = 500 \text{ N/m}^2$  was considered. Figure 9 shows the time histories of the vertical displacement at four points of the soil-foundation interface (Figure 7.(d)). Points  $A^s$  and  $B^s$  were located at the soil surface, and points  $A^f$  and  $B^f$  belonged to the foundation. In all points of the interface, displacement compatibility was satisfied while the load was applied. Although a gap appeared in the non-linear response when the load was withdrawn, it became negligible as the inertia forces decreased.

The dynamic behaviour of the soil and the foundation in the antisymmetrical load case is shown in Figure 10. In this load case, differences between the linear and non-linear response were noticeable. Because

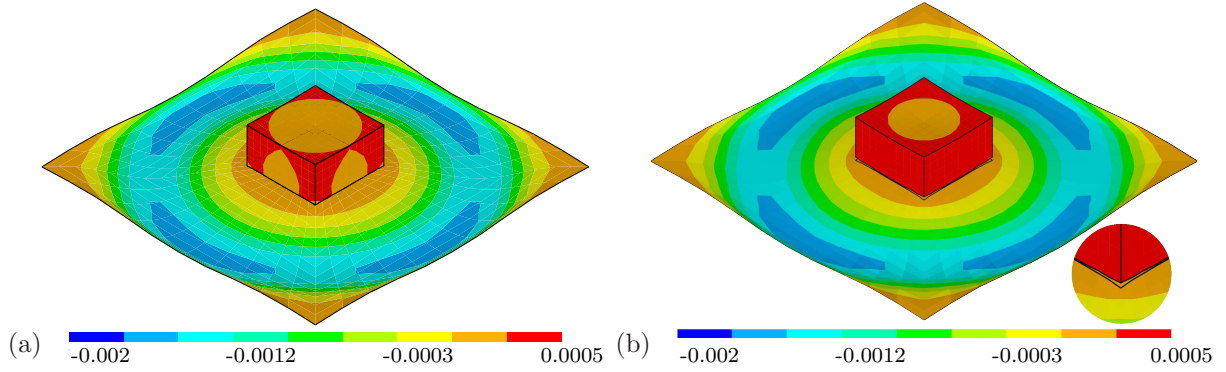


Figure 8: Dimensionless dynamic response  $\tilde{u} = \pi \mu u(t) r / p_0$  of the soil-foundation system in the symmetrical load case accounting for (a) linear and (b) non-linear contact.

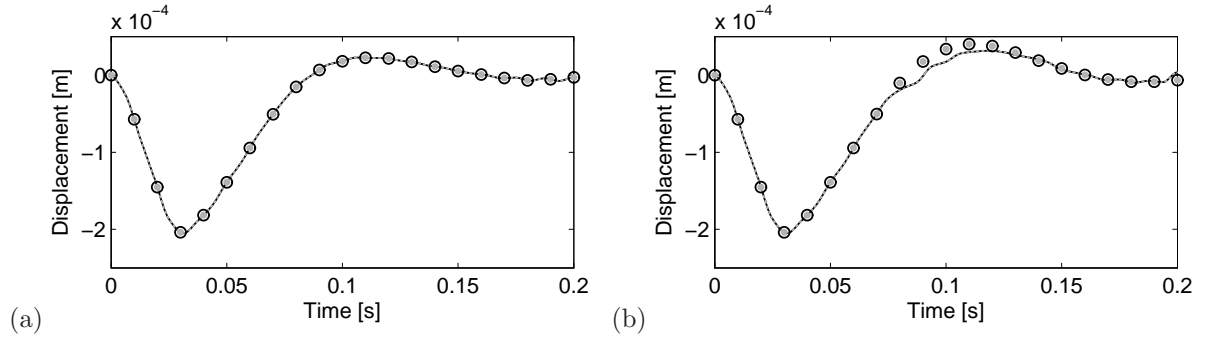


Figure 9: Time history of the vertical displacement at the soil-foundation interface at  $A^s$  (grey dotted line),  $A^f$  (grey dots),  $B^s$  (black solid line) and  $B^f$  (black circles) in the symmetrical load case accounting for (a) linear and (b) non-linear contact.

of non-linear effects, displacement compatibility was not satisfied in one half of the soil-structure interface. The time histories of the vertical displacement at the interface are shown in Figure 11. The linear problem presented an antisymmetrical response that was lost when non-linear contact was taken into account. As regards the linear problem, the minimum displacement at point  $B^s$  increased and the maximum displacement at point  $A^s$  decreased since soil and foundation were separated. However, the maximum displacement at point  $A^f$  increased because this area of the foundation did not pull the soil.

### 5.2. Dynamic response of a structure to an incident wave field

This section analyses the dynamic response of a structure to a wave field induced by an impulsive load. Figure 12 shows a drawing of the building and the load case considered. The dimensions of the three-storey building were  $14.4 \text{ m} \times 10.8 \text{ m} \times 9 \text{ m}$ . The structure consisted of concrete columns and beams with  $0.5 \text{ m} \times 0.5 \text{ m}$  and  $0.3 \text{ m} \times 0.5 \text{ m}$  sections, respectively. The floors were simply supported concrete slabs with a thickness of  $0.3 \text{ m}$  and a mass per unit area of  $330 \text{ kg/m}^2$ . Masses of non-structural elements (e.g. partition and other walls, tiles) were considered to amount to  $100 \text{ kg/m}^2$  on the floors,  $220 \text{ kg/m}^2$  on the roof and

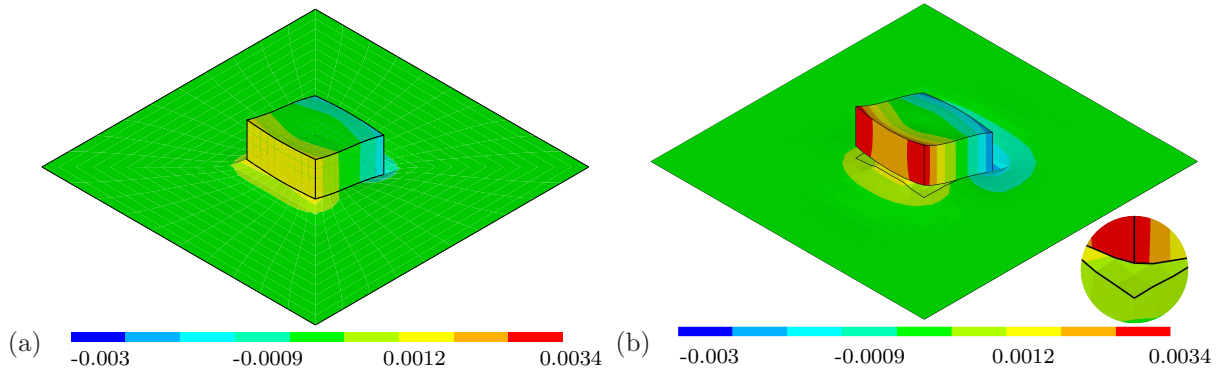


Figure 10: Dimensionless dynamic response  $v = \pi\mu u(t)r/p_0$  of the soil-foundation system in the antisymmetrical load case accounting for (a) linear and (b) non-linear contact.

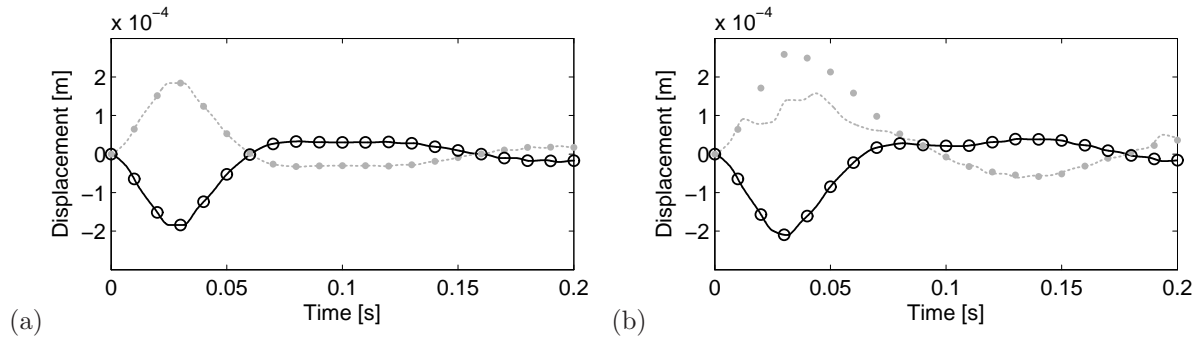


Figure 11: Time history of the vertical displacement at the soil-foundation interface at  $A^s$  (grey dotted line),  $A^f$  (grey dots),  $B^s$  (black solid line) and  $B^f$  (black circles) in the antisymmetrical load case accounting for (a) linear and (b) non-linear contact.

918 kg/m and 486 kg/m on the exterior and interior beams, respectively. The structure was founded on a 0.5 m thick concrete slab. The concrete had the following properties: Young's modulus  $E = 30 \times 10^9 \text{ N/m}^2$ , Poisson's ratio  $\nu = 0.2$  and density  $\rho = 2500 \text{ kg/m}^3$ . The structural response was governed by dynamic soil-structure interaction effects. The soil was represented as an elastic half-space with the following properties:  $c_p = 208 \text{ m/s}$ ,  $c_s = 100 \text{ m/s}$ ,  $c_R = 93 \text{ m/s}$  and  $\rho = 1800 \text{ kg/m}^3$ .

Figure 13 shows the discretization of the soil-structure system. The soil was discretized by using 398 quadrilateral nine-node boundary elements 18 m around the building. The structure was considered by 1176 two-node beam elements and 1728 four-node shell elements.

The building was affected by a wave field induced by an impulsive load  $p(t)$  applied 14.5 m from the structure, where  $p(t) = p_0(H(t) - H(t - 0.025, s))$  with  $p_0 = 1000 \text{ N/m}^2$ . The time step for the analysis was set at  $\Delta t = 5 \times 10^{-3} \text{ s}$ . The stability parameter  $\beta = c_s \Delta t / l$  took values  $0.4 < \beta < 1.2$ . To reduce computational effort, the influence matrices were interpolated from  $T_L = 0.27 \text{ s}$  by  $k = 20$  interpolating matrices using a Chebyshev-Lagrange approach. Once the initial settings were done, the running time to

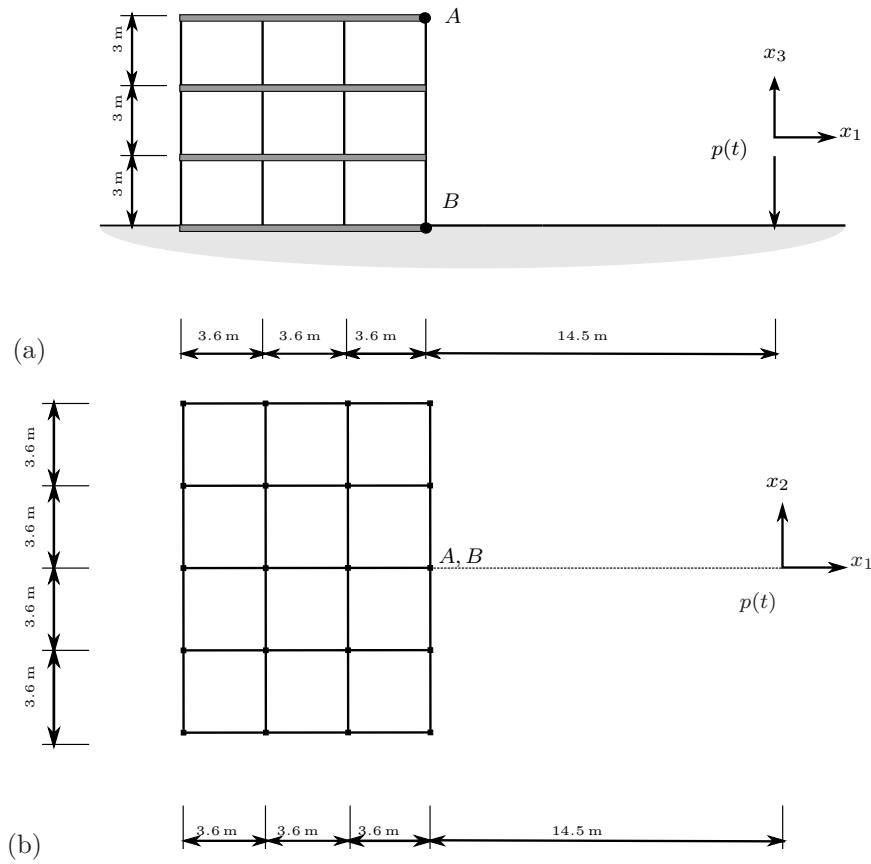


Figure 12: Building geometry and load case: (a) elevation and (b) plan.

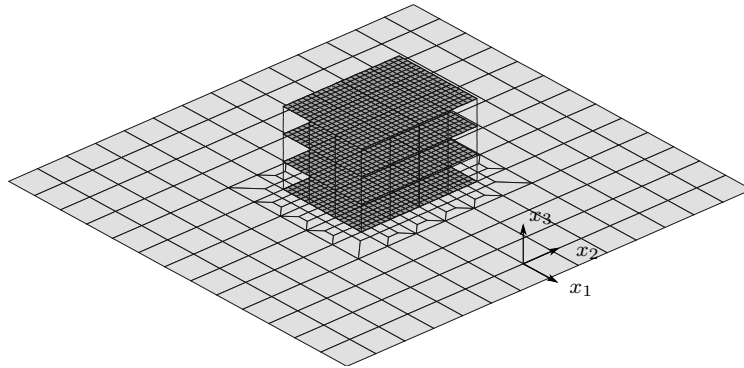


Figure 13: Soil and building discretization.

solve this problem was approximately 1 hour.

Figure 14 shows translational mode shapes of the structure according to the direction of wave propagation  $x_1$  and mode shapes associated with slab bending. Torsional and  $x_2$  translational mode shapes are not shown. To compute these mode shapes, soil-structure interaction was neglected. The same structural damping

$\zeta = 2\%$  was considered for all modes that contributed significantly to the response of the structure, shown in Figure 14 [53]. A value of  $\alpha_m = 0.68 \text{ s}^{-1}$  was obtained.

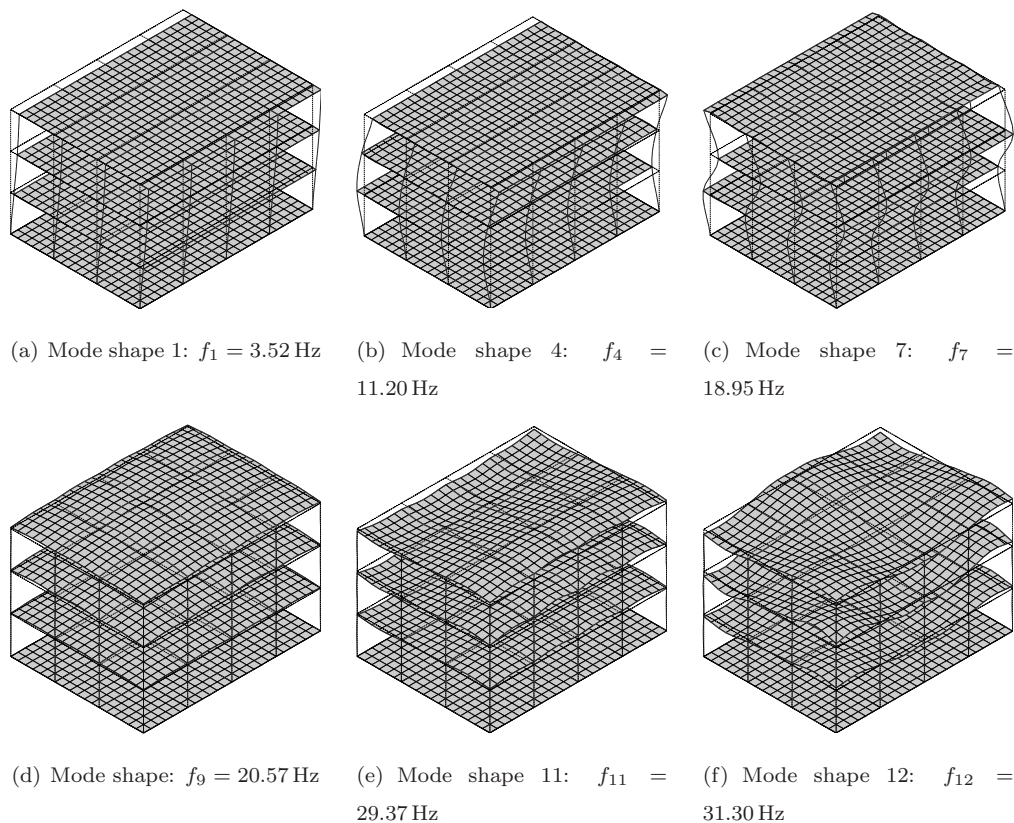


Figure 14: Translational and slab bending mode shapes. SSI is not considered.

Figure 15 shows the dimensionless response  $\tilde{u} = \pi\mu u(t)r/p_0$  of the soil-foundation system at time  $t = 0.35 \text{ s}$ , where  $r$  is the distance between the observation point and the load. The incident wave field induces a deformation of the foundation that is transmitted along the structure. Soil-foundation interaction leads to higher free field displacements than soil-foundation interface displacements due to the foundation's stiffness.

Figure 16 shows the time history and frequency content of the  $x_1$  in-plane and vertical acceleration at two points of the building. The dynamic response of the upper floor was greater than that of the foundation. Both vertical responses were in phase but the horizontal responses had a different phase due to the translational mode shapes. The response was attenuated once the incident wave crossed the building. The frequency content shows peaks associated with the resonance frequencies  $\tilde{f}_1 = 3.09 \text{ Hz}$ ,  $\tilde{f}_4 = 10.48 \text{ Hz}$ ,  $\tilde{f}_7 = 17.70 \text{ Hz}$ ,  $\tilde{f}_9 = 19.76 \text{ Hz}$ ,  $\tilde{f}_{11} = 28.01 \text{ Hz}$  and  $\tilde{f}_{12} = 29.73 \text{ Hz}$ . These frequencies are slightly lower than those presented in Figure 14 because soil-structure interaction was taken into account.

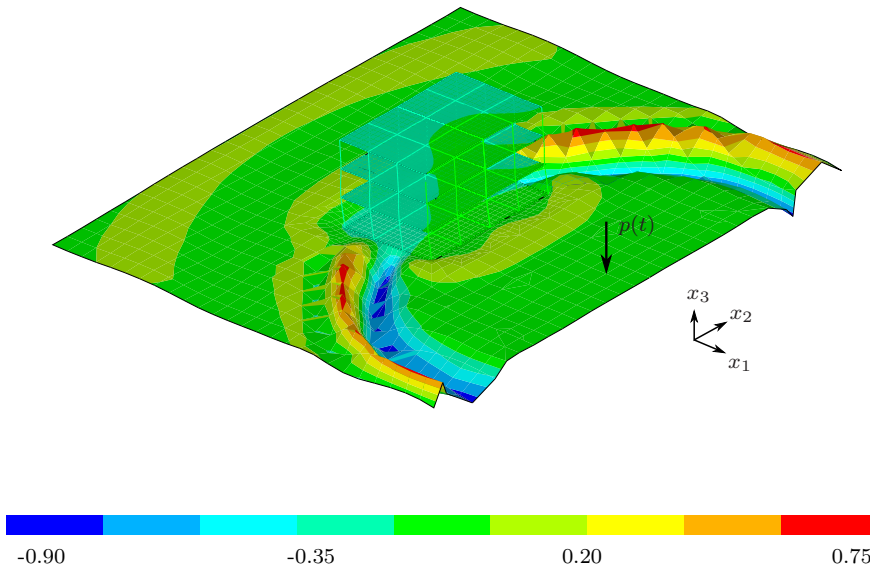


Figure 15: Dimensionless dynamic soil-structure response  $\tilde{u} = \pi\mu u(t)r/p_0$  at  $t = 0.35$  s.

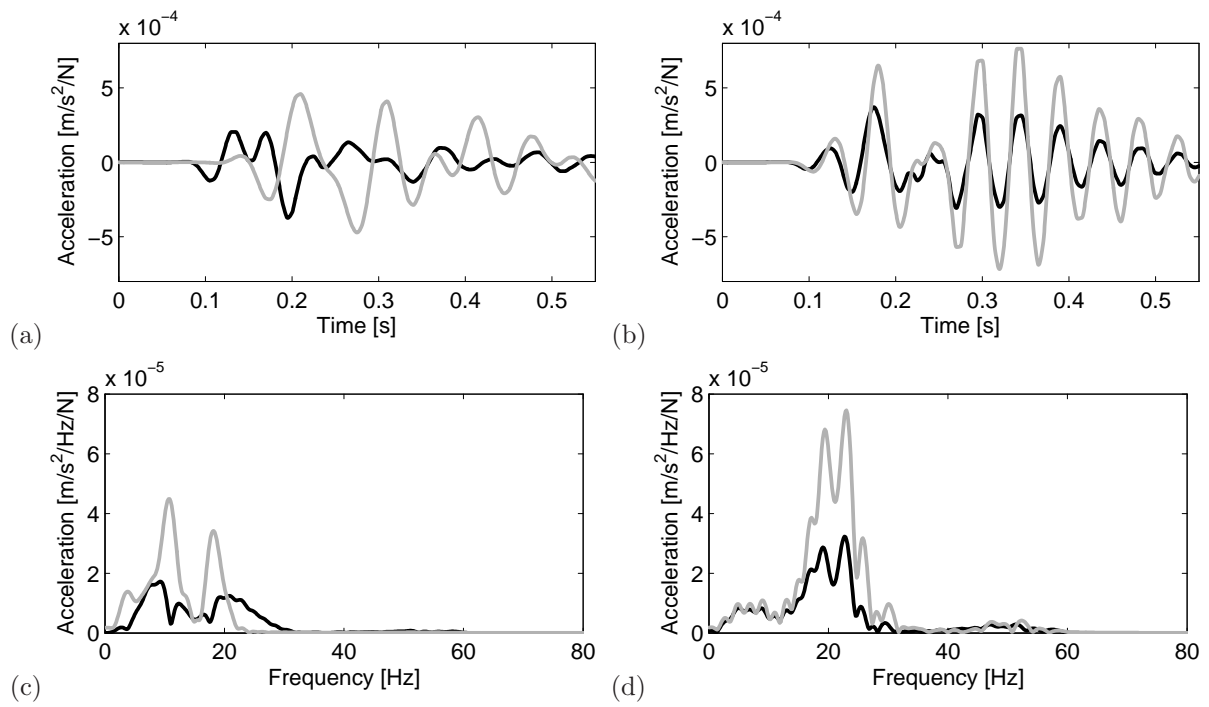


Figure 16: (a,b) Time history and (c,d) frequency content of the (a,c) in-plane and (b,d) vertical acceleration at A (grey line) and B (black line).

## 6. Conclusions

This paper analysed the need for a 3D non-linear time domain FEM-BEM numerical model studying two soil-structure interaction problems. The BEM formulation was improved by using interpolation matrices to

compute time-domain influence matrices. The FEM approach was based on implicit Green's functions.

In the first example, the propagation of waves in an elastic foundation on a homogeneous soil was analysed accounting for linear and non-linear contact effects. A comparison of the computed results shows that the problem requires including non-linear behaviour to represent any uplifting or other effects.

In the second example, the dynamic response of a structure to an incident wave field was considered. The proposed methodology made it possible to rigorously account for soil-structure interaction. In this example, non-linear contact effects were not noticeable.

The proposed model is limited to linear and elastic soil behaviour. Problems that involve estimations of the initial states of stress in soils and of the changes in these stresses during loading, e.g. studies of settlements under conditions in which the induced stress varies spatially, could not be analysed.

## Acknowledgments

This research was funded by the Spanish Ministry of Science and Innovation (*Ministerio de Ciencia e Innovación*) through research project BIA2010-14843. Financial support is gratefully acknowledged. The authors also wish to acknowledge the support provided by the Andalusian Scientific Computing Centre (CICA).

## References

- [1] J. Domínguez, *Boundary elements in dynamics*, Computational Mechanics Publications and Elsevier Applied Science, Southampton, 1993.
- [2] J. Domínguez, *Response of embedded rectangular foundations to travelling waves*, Tech. rep., Department of Civil Engineering, R78-24, Cambridge, Massachusetts, USA (1978).
- [3] K.-L. Fok, A.K. Chopra, [Frequency response functions for arch dams: hydrodynamic and foundation flexibility effects](#), *Earthquake Engineering & Structural Dynamics* 14 (5) (1986) 769–795.
- [4] F. Medina, J. Domínguez, J.L. Tassoulas, [Response of dams to earthquakes including effects of sediments](#), *Journal of Structural Engineering*, New York N.Y. 116 (11) (1990) 3108–3121.
- [5] J.J. Aznárez, O. Maeso, J. Domínguez, [BE analysis of bottom sediments in dynamic fluid-structure interaction problems](#), *Engineering Analysis with Boundary Elements* 30 (2) (2006) 124–136.
- [6] A.M. Kaynia, E. Kausel, [Dynamics of piles and pile groups in layered soil media](#), *Soil Dynamics and Earthquake Engineering* 10 (8) (1991) 386–401.
- [7] S. François, L. Pyl, H.R. Masoumi, G. Degrande, [The influence of dynamic soil-structure interaction on traffic induced vibrations in buildings](#), *Soil Dynamics and Earthquake Engineering* 31416 (27) (2007) 655–674.
- [8] L.A. Padrón, J.J. Aznárez, O. Maeso, [Dynamic structure-soil-structure interaction between nearby piled buildings under seismic excitation by BEM-FEM model](#), *Soil Dynamics and Earthquake Engineering* 29 (6) (2009) 1084–1096.
- [9] L. Auersch, [Wave propagation in the elastic half-space due to an interior load and its application to ground vibration problems and buildings on pile foundations](#), *Soil Dynamics and Earthquake Engineering* 30 (10) (2010) 925–936.
- [10] X. Sheng, D.J. Thompson, C.J.C. Jones, G. Xie, S.D. Iwnicki, P. Allen, S.S. Hsu, [Simulations of roughness initiation and growth on railway rails](#), *Journal of Sound and Vibration* 293 (3-5) (2006) 819–829.

- [11] [G. Lombaert, G. Degrande, J. Kogut, S. François, The experimental validation of a numerical model for the prediction of railway induced vibrations, \*Journal of Sound and Vibration\* 297 \(3-5\) \(2006\) 512–535.](#)
- [12] [L. Auersch, The effect of critically moving loads on the vibrations of soft soils and isolated railway tracks, \*Journal of Sound and Vibration\* 310 \(3\) \(2008\) 587–607.](#)
- [13] [D.E. Beskos, Boundary element methods in dynamic analysis: Part II \(1986-1996\), \*Applied Mechanics Reviews\* 50 \(3\) \(1997\) 149–197.](#)
- [14] [W.J. Mansur, A time-stepping technique to solve wave propagation problems using the boundary element method, Ph.D. thesis, University of Southampton, UK \(1983\)](#)
- [15] [D.L. Karabalis, D.E. Beskos, Dynamic response of 3-D rigid surface foundations by time domain boundary element method, \*Earthquake Engineering & Structural Dynamics\* 12 \(1\) \(1984\) 73–93.](#)
- [16] [D.L. Karabalis, D.E. Beskos, Dynamic response of 3-D flexible foundations by time domain BEM and FEM, \*International Journal of Soil Dynamics and Earthquake Engineering\* 4 \(2\) \(1985\) 91–101.](#)
- [17] [D.-P.N. Kontoni, D.E. Beskos, G.D. Manolis, Uniform half-plane elastodynamic problems by an approximate boundary element method, \*Soil Dynamics and Earthquake Engineering\* 6 \(4\) \(1987\) 227–238.](#)
- [18] [M. Schanz, Application of 3D time domain boundary element formulation to wave propagation in poroelastic solids, \*Engineering Analysis with Boundary Elements\* 25 \(4-5\) \(2001\) 363–376.](#)
- [19] [D.C. Rizos, Z. Wang, Coupled BEM-FEM solutions for direct time domain soil-structure interaction analysis, \*Engineering Analysis with Boundary Elements\* 26 \(10\) \(2002\) 877–888.](#)
- [20] [J. O'Brien, D.C. Rizos, A 3D BEM-FEM methodology for simulation of high speed train induced vibrations, \*Soil Dynamics and Earthquake Engineering\* 25 \(4\) \(2005\) 289–301.](#)
- [21] [M. Marrero, J. Domínguez, Numerical behavior of time domain BEM for three-dimensional transient elastodynamic problems, \*Engineering Analysis with Boundary Elements\* 27 \(1\) \(2003\) 39–48.](#)
- [22] [P. Galvín, J. Domínguez, Analysis of ground motion due to moving surface loads induced by high-speed trains, \*Engineering Analysis with Boundary Elements\* 31 \(11\) \(2007\) 931–941.](#)
- [23] [P. Galvín, A. Romero, J. Domínguez, Fully three-dimensional analysis of high-speed train-track-soil-structure dynamic interaction, \*Journal of Sound and Vibration\* 329 \(24\) \(2010\) 5147–5163.](#)
- [24] [P. Galvín, A. Romero, J. Domínguez, Vibrations induced by HST passage on ballast and non-ballast tracks, \*Soil Dynamics and Earthquake Engineering\* 30 \(9\) \(2010\) 862–873.](#)
- [25] [A. Romero, M. Solís, J. Domínguez, P. Galvín, Soil-structure interaction in resonant railway bridges, \*Soil Dynamics and Earthquake Engineering\* \(2012\), <http://dx.doi.org/10.1016/j.soildyn.2012.07.014>.](#)
- [26] [T.J.R. Hughes, Analysis of transient algorithms with particular reference to stability behavior, In: T. Belytshcko, T.J.R. Hughes, editors. \*Computational methods for transient analysis\*. North Holland: Elsevier, 1983.](#)
- [27] [A. Frangi, G. Novati, On the numerical stability of time-domain elastodynamic analyses by BEM, \*Computer Methods in Applied Mechanics and Engineering\* 173 \(3-4\) \(1999\) 403–417.](#)
- [28] [W.J. Mansur, C.A. Brebbia, Transient elastodynamics using a time-stepping technique, \*Boundary Elements \(C. Brebbia, et al. Eds.\)\*, Springer-Verlag, Berlin and CML publications Southampton, 1983.](#)
- [29] [F.C. Araújo, W.J. Mansur, L.K. Nishikava, Linear  \$\theta\$  time-marching algorithm in 3D BEM formulation for elastodynamics, \*Engineering Analysis with Boundary Elements\* 23 \(10\) \(1999\) 825–833.](#)
- [30] [G. Yu, W.J. Mansur, J.M.A. Carrer, L. Gong, A linear  \$\theta\$  method applied to 2D time-domain BEM, \*Communications in Numerical Methods in Engineering\* 14 \(12\) \(1998\) 1171–1179.](#)
- [31] [G. Yu, W.J. Mansur, J.M.A. Carrer, L. Gong, Time weighting in time domain BEM, \*Engineering Analysis with Boundary Elements\* 22 \(3\) \(1998\) 175–181.](#)
- [32] [A.P. Peirce, E. Siebrits, Stability analysis and design of time-stepping schemes for general elastodynamic boundary element](#)

- models, *International Journal for Numerical Methods in Engineering* 40 (2) (1997) 319–342.
- [33] B. Birgisson, E. Siebrits, A.P. Peirce, [Elastodynamic direct boundary element methods with enhanced numerical stability properties](#), *International Journal for Numerical Methods in Engineering* 46 (6) (1999) 871–888.
- [34] C.C. Spyrakos, D.E. Beskos, [Dynamic response of flexible strip-foundations by boundary and finite elements](#), *Soil Dynamics and Earthquake Engineering* 5 (2) (1986) 84–96.
- [35] M.J. Prabucki, O. von Estorff, [Dynamic response in the time domain by coupled boundary and finite elements](#), *Computational Mechanics* 6 (1) (1990) 35–46.
- [36] O. von Estorff, [Coupling of BEM and FEM in the time domain: Some remarks on its applicability and efficiency](#), *Computers and Structures* 44 (1-2) (1992) 325–337.
- [37] O. von Estorff, C. Hagen, [Iterative coupling of FEM and BEM in 3D transient elastodynamics](#), *Engineering Analysis with Boundary Elements* 30 (7) (2006) 611–622.
- [38] D. Soares Jr., O. von Estorff, W.J. Mansur, [Iterative coupling of BEM and FEM for nonlinear dynamic analyses](#), *Computational Mechanics* 34 (1) (2004) 67–73.
- [39] W.M. Elleithy, H.J. Al-Gahtani, M. El-Gebeily, [Iterative coupling of BE and FE methods in elastostatics](#), *Engineering Analysis with Boundary Elements* 25 (8) (2001) 685–695.
- [40] M. El-Gebeily, W.M. Elleithy, H.J. Al-Gahtani, [Convergence of the domain decomposition finite element-boundary element coupling methods](#), *Computer Methods in Applied Mechanics and Engineering* 191 (43) (2002) 4851–4867.
- [41] W.M. Elleithy, M. Tanaka, [Interface relaxation algorithms for BEM-BEM coupling and FEM-BEM coupling](#), *Computer Methods in Applied Mechanics and Engineering* 192 (26-27) (2003) 2977–2992.
- [42] D. Soares Jr., W.J. Mansur, O. von Estorff, [An efficient time-domain FEM/BEM coupling approach based on FEM implicit Green’s functions and truncation of BEM time convolution process](#), *Computer Methods in Applied Mechanics and Engineering* 196 (9-12) (2007) 1816–1826.
- [43] A.F. Teles da Silva, D.H. Peregrine, [Nonlinear perturbations on a free surface induced by a submerged body: A boundary integral approach](#), *Engineering Analysis with Boundary Elements* 7 (4) (1990) 214–222.
- [44] D. Soares Jr., W.J. Mansur, [Compression of time-generated matrices in two-dimensional time-domain elastodynamic BEM analysis](#), *International Journal for Numerical Methods in Engineering* 61 (8) (2004) 1209–1218.
- [45] D. Soares, W.J. Mansur, [A time domain FEM approach based on implicit Green’s functions for non-linear dynamic analysis](#), *International Journal for Numerical Methods in Engineering* 62 (5) (2005) 664–681.
- [46] D. Soares Jr., [An optimised FEM-BEM time-domain iterative coupling algorithm for dynamic analyses](#), *Computers and Structures* 86 (19-20) (2008) 1839–1844.
- [47] D. Soares Jr., [Fluid-structure interaction analysis by optimised boundary element-finite element coupling procedures](#), *Journal of Sound and Vibration* 322 (1-2) (2009) 184–195.
- [48] P. Wriggers, [Computational Contact Mechanics](#), 2nd Edition, Springer, 2006.
- [49] F. Hartmann, [Coupling C-Matrix in Non-smooth Boundary Points](#), in *New Developments in Boundary Elements Methods*, Brebbia CA. (ed), Butterworths, 1980.
- [50] F. Hartmann, [The somigliana identity on piecewise smooth surfaces](#), *Journal of Elasticity* 11 (1981) 403–423.
- [51] C.L. Pekeris, [The seismic surface pulse](#), *Proceedings of the National Academy of Sciences of the United States of America* 41 (1955) 469–480.
- [52] D.C. Rizos, D.L. Karabalis, [A time domain BEM for 3-D elastodynamic analysis using the B-spline fundamental solutions](#), *Computational Mechanics* 22 (1) (1998) 108–115.
- [53] R.W. Clough, J. Penzien, [Dynamic of Structures](#), McGraw-Hill, New York, 1975.
- [54] M. Schanz, [Wave propagation in Viscoelastic and Poroelastic Continua: A Boundary Element Approach](#), Springer, Berlin, 2001.

- [55] R. Abascal, 2D transient dynamic friction contact problems II. Applications to soil-structure interaction problems, *Engineering Analysis with Boundary Elements* 16 (3) (1995) 235–243.